Internal Electric Field and Second-Order Optical Nonlinearity of Ferroelectric Nylon 11

Naoto Tsutsumi,* Toru Mizutani, and Wataru Sakai

Department of Polymer Science & Engineering, Kyoto Institute of Technology, Matsugasaki, Sakyo, Kyoto 606, Japan

Received September 17, 1996; Revised Manuscript Received January 21, 1997[⊗]

ABSTRACT: This paper presents ferroelectric polarization reversal, internal electric field and second harmonic generation for cold-drawn Nylon 11 films. The draw ratio is between 2.6 and 2.8. Clear polarization reversal for cold-drawn Nylon 11 films can be measured when films are subjected to the sinusoidal applied field at room temperature. The internal electric field created by the aligned dipoles is measured by the spectrum shift and broadening of electrochromic dye. An internal electric field in the order of MV/cm is obtained, which is proportional to the remanent polarization. Second-order optical nonlinearity is measured from the Maker fringe second harmonic generation measurement. Drawn and poled polymer films belong to the $mm2$ point group and have second-order optical nonlinearity with three different tensor components, d_{31}, d_{32}, and d_{33}. The second harmonic generation coefficients, d_{33} and d_{31}, increase with increasing remanent polarization, whereas the value of d_{32} is nearly zero irrespective of the intensity of the remanent polarization. The average ratio between d_{33} and d_{31} is 3.8.

Introduction

Ferroelectricity of vinylidene fluoride polymers has been of great interest because of the polarization reversal and the existence of ferroelectric to paraelectric transition. Polarization reversals of poly(vinylidene fluoride) (PVDF)[1] and copolymer of vinylidene fluoride and trifluoroethylene (P(VDF-TrFE))[2] originate from the cooperative switching of β-crystallite dipoles. A clear Curie transition temperature at which the transition from ferroelectric to paraelectric phases occurs was measured in P(VDF-TrFE).[2] Recently the polarization reversal of the aliphatic polyamides of Nylons 11 and 7[3,4] and the aromatic−aliphatic polyamide[5,6] have also been investigated.

We have studied the internal electric field created by the aligned β-crystallite dipoles for P(VDF-TrFE),[7] the blend of PVDF and poly(methyl methacrylate) (PMMA),[8] and the P(VDF-TrFE)/PMMA blend.[9] Furthermore, the internal electric field created by the amorphous dipoles in aromatic−aliphatic polyamide films has been investigated.[6] The internal electric field is measured using the electrochromic spectrum change of probe molecules dispersed in the matrix. The internal electric field is on the order of MV/cm depending on the achieved polarization, which was a few times larger than the poling field. Furthermore the second-order optical nonlinearity was measured for P(VDF-TrFE)/PMMA blends[9] and NLO dye dispersed PVDF/PMMA blends.[10]

Recently, we have found that cold-drawn and poled Nylon 11 films show a large internal electric field created by the aligned crystallite dipoles and second-order optical nonlinearity with three different tensor components. Internal electric field is measured by the absorption spectrum change of the electrochromic probe dye dispersed in the Nylon 11 matrix. In this study, we have investigated the internal electric field and second-order optical nonlinearity for cold-drawn and poled Nylon 11 films, which are related to the remanent polarization measured by ferroelectric polarization reversal.

* To whom correspondence should be addressed.
[⊗] Abstract published in *Advance ACS Abstracts,* March 1, 1997.

Experimental Section

Sample Preparation. Nylon 11 (Aldrich Chemical Co.) was used as received. 4-(Dimethylamino)-4′-nitrostilbene (DANS) (Eastman Kodak Co.) was recrystallized from amyl alcohol and dried at 50−60 °C in vacuo. To incorporate DANS in Nylon 11, Nylon 11 (1 g) and DANS (1 mg) were dissolved in a hexafluoro-2-propanol (8 mL) and cast at room temperature for 24 h followed by drying at 40−50 °C for 6−8 h. Nylon 11 and Nylon 11 with DANS films were melt-pressed between Upilex polyimide films at 210 °C on a heated press to thickness of ca. 40−60 μm. The molten films were quenched into liquid nitrogen. Neat Nylon 11 films were drawn by 2.8 times and DANS/Nylon 11 films by 2.6 times at room temperature to a thickness of 30−40 μm.

Electrical and Optical Measurements. A 0.05 Hz sinusoidal voltage was applied for 1 h at room temperature to the aluminum electrodes, which had been evaporated onto opposing surfaces of the films, in a 3M-produced inert liquid, Fluorinert FC40. Poling current was monitored during application of the voltage and was used to calculate the remanent polarization, allowing for impedance losses.[11,12] The pyroelectric coefficient (C_{pyro}) was determined by measuring the current generated upon heating and cooling the poled film at a measured rate of 1−2 °C/min in the vicinity of 30 °C. Ultraviolet−visible spectra of the films were measured in transmission on a UV−vis spectrometer after the aluminum electrodes were removed by immersing them in 10 wt % sodium hydroxide solution for a few minutes. A prism coupling method was employed to measure the refractive indices of materials. Laser sources are a polarized He−Ne laser (632.8 nm) and a laser diode (830 nm). The prism of TaFD21 (HOYA Glass) with high refractive index (1.925 88 at 632.8 nm), and the film was coupled with an air gap. The critical angle at which a complete reflection changes to partial reflection, i.e. part of the light penetrates into the bulk film, was measured to determine the refractive indices, since the film thickness is approximately 20 μm.

Second Harmonic Generation Measurements. The Maker fringe method is employed to measure the second harmonic generation (SHG) intensity of poled spun-cast films. All SHG measurements were carried out for the sample films without DANS. The laser source is a Continuum Model Surelite-10 Q-switched Nd:YAG pulse laser with 1064 nm *p*- or *s*-polarized fundamental beam (320 mJ maximum energy, 7 ns pulse width, and 10 Hz repeating rate). The generated second harmonic (SH) wave was detected by a photomultiplier. The SH signal averaged on a gated integrator and boxcar averager module was transferred to a microcomputer through

S0024-9297(96)01385-X CCC: $14.00

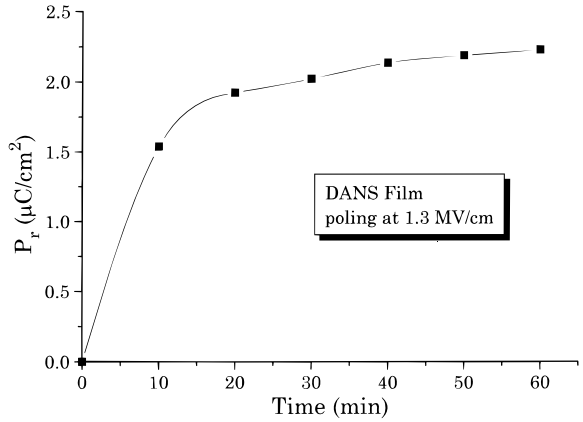

Figure 1. Dependence of poling time on P_r. Poling field is 1.3 MV/cm.

a computer interface module. The detailed experimental procedure is described in refs 9 and 10.

Characterization. WAXS patterns of the films were measured on a X-ray diffractometer with nickel-filtered Cu Kα radiation.

Results and Discussion

Polymer Structure. WAXS profiles show that melt-quenched and drawn sample has the intensity maximum at the angle (2θ) around 21.0° ascribed to the δ'-crystallite phase.[13] The crystallite size of the δ'-crystal, 52.7 Å, was estimated from the half-width and peak position using a Scherrer relation. A previous work[4] reported that annealing gave rise to difficulty in dipole switching and the resultant decrease of ferroelectricity in Nylons 7 and 11 films. Therefore, no thermal annealing was performed for the present film preparation process.

Polarization Current and Polarization Charge. The polarization current and its time integral (polarization charge) for the drawn film were measured as a function of sinusoidal applied electric field with various maximum field at room temperature. A clear and large polarization current is observed, which can be compared with that for P(VDF-TrFE).[7] Current flows on the external circuit are the summation of the currents due to the polarization, capacitance, and conductivity,[12] i.e.

$$J = J_D + J_\rho = \frac{dP}{dt} + \epsilon\epsilon_0\frac{dE_p}{dt} + \frac{E}{\rho} \qquad (1)$$

where J is the poling current, J_D is displacement current, J_ρ is conduction current, ϵ is relative permittivity, ϵ_0 is permittivity of vacuum, P is polarization, E_p is applied electric field, and ρ is resistivity. Polarization current is the poling current reduced by the terms of capacitance and conductivity. In the polarization charge profile, the remanent polarization (P_r) is the value of polarization at zero applied field and the coercive field (E_c) is the applied field at zero polarization after the last cycle of poling. E_c values were in the range 0.5−0.6 MV/cm. The dependence of P_r on poling time is shown in Figure 1. The maximum poling field is 1.3 MV/cm. The P_r value largely increased at 10 min of sinusoidal poling and almost levels out at 60 min of poling. The time of 60 min is enough to obtain the maximum P_r value at that poling field.

Internal Electric Field, Remanent Polarization, and Pyroelectricity. The internal electric field (E_i) which is created by the aligned dipole moments was measured by the spectrum change of the probe molecule

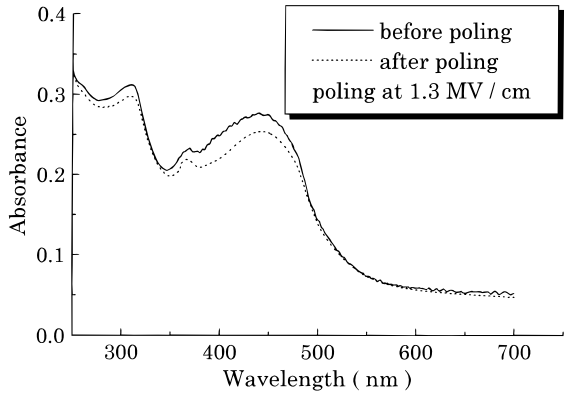

Figure 2. UV−vis absorption spectra of DANS before and after poling at 1.3 MV/cm.

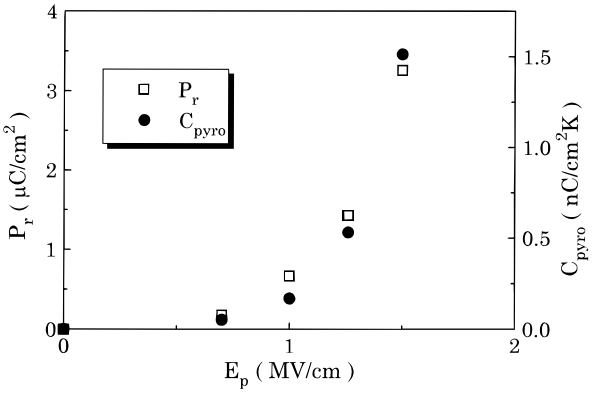

Figure 3. Plots of P_r and C_{pyro} as a function of E_p.

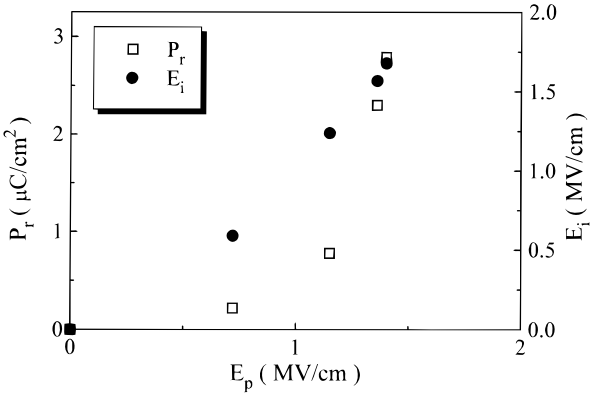

Figure 4. Plots of P_r and E_i as a function of E_p.

of DANS dispersed in the Nylon 11 matrix, using the electrochromic theory.[14,15] As we did before,[7−9] the difference between the absorption spectra before and after poling can be expressed as a Taylor series expansion with first, second, and higher orders of the derivatives of the unperturbed spectrum (spectrum before poling). The detailed derivation and calculation are expressed in our previous literatures of refs 7 and 9. Figure 2 shows the UV−vis absorption spectra of DANS in the films before and after poling. Poling causes a decrease of intensity due to orientation of DANS to the film thickness and the spectrum red shift and broadening due to the change of electronic state by the internal electric field.

An increase of the maximum applied field leads to a larger remanent polarization and coercive field, which is the same as in the case of P(VDF-TrFE).[7] Figures 3 and 4 show the plots of P_r and C_{pyro} and the plots of P_r and E_i, respectively, when a maximum applying field

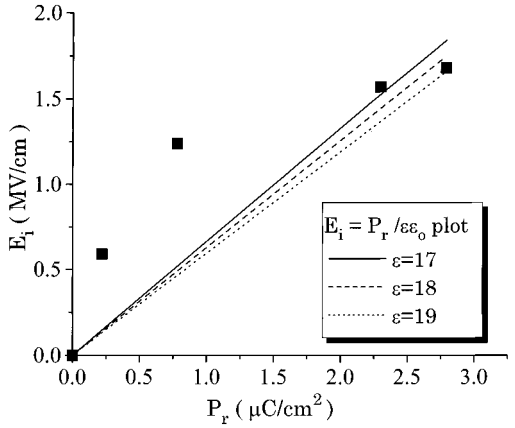

Figure 5. Plots of P_r vs E_i. The relation of $E_i = (P_r/\epsilon\epsilon_0)$ is plotted with $\epsilon = 17$ (solid line), $\epsilon = 18$ (dashed line), and $\epsilon = 19$ (dotted line).

Table 1. RI Values at Wavelengths of 632.8 and 830 nm Measured and Those at 532 and 1064 nm Predicted by Eq 2

	wavelength (nm)			
	632.8	830	532	1064
n_x	1.539	1.535	1.543	1.533
n_y	1.508	1.503	1.514	1.501
n_z	1.498	1.493	1.503	1.491

(E_p) is changed. As shown in Figure 3, P_r and C_{pyro} nonlinearly increase with increasing E_p. As shown in Figure 4, E_i values also increase with increasing E_p. As discussed in our previous paper for the PVDF/PMMA blend,[8] the nonlinear dependence is ascribed to an increase in the ratio of crystallite/amorphous polarization with increasing E_p. The sample of interest consists of amorphous and crystalline phases. The electric field subjected to the two phases is not the same because the amorphous and crystalline phases have respective different relative permittivities. At higher E_p, the crystallite polarization is expected to contribute importantly to P_r, C_{pyro}, and E_i. In Figure 5, E_i is plotted as a function of P_r. As discussed in our previous paper for the internal electric field created by the aligned β-crystallite dipoles of P(VDF-TrFE),[7] the polarization charges produce the internal electric field within the amorphous regions of the polymer matrix where DANS dyes reside. The electric field within such regions might be expected to be $(P_r/\epsilon\epsilon_0)$.[16] The lines drawn through the origin in the figure are those with a slope of $(1/\epsilon\epsilon_0)$ where $\epsilon = 17$ (solid line), $\epsilon = 18$ (dashed line), and $\epsilon = 19$ (dotted line). These relative permittivities were obtained from the analysis of the polarization current using eq 1. At the P_r region higher than 2.0 μC/cm^2, the $P_r - E_i$ profile is well fitted by the relation of $E_i = (P_r/\epsilon\epsilon_0)$. However, in the relatively lower P_r region, E_i is higher than the value expected from the relation. This might be attributed to the space charges injected from the electrode when the sample is sinusoidally poled.

Refractive Indices. The refractive indices (RI) for transverse electric field (TE) and transverse magnetic field (TM) modes are measured using a prism-coupling method at wavelength of 632.8 and 830 nm. TM mode measurement provides the RI value along the direction of film thickness, and the TE mode measurement gives the RI value in the plane of film. RI values at wavelength of 632.8 and 830 nm were listed for the unpoled polymer films in Table 1. Vector configuration of refractive indices, n_x, n_y, and n_z is shown in Figure 6. Here n_x, n_y, and n_z are RI values along the drawing direction, perpendicular to the drawing direction in plane of film, and in the poling direction parallel to film thickness direction, respectively. A large anisotropy of $n_x > n_y > n_z$ is measured, and the anisotropy originates from the alignment of polymer chain along the drawing direction. The largest refractive index, n_x, is obtained along the drawing direction and the smallest one, n_z, is obtained in the direction of the film thickness, perpendicular to the surface plane of the films. The wavelength dispersion of RI, $n_f(\lambda)$, can be fitted to a one-oscillator Sellmeier-dispersion formula

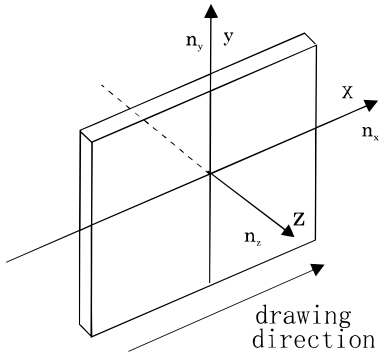

Figure 6. Refractive indices configuration.

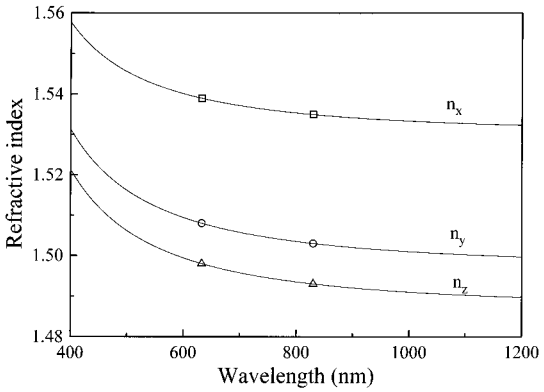

Figure 7. Plots of RI at wavelengths of 632.8 and 830 nm and the predicted plot curve of the wavelength dispersion of RI using eq 2.

$$n_f^2(\lambda) - 1 = \frac{q}{1/\lambda_0^2 - 1/\lambda^2} + A \qquad (2)$$

where λ_0 is the absorption wavelength of the dominant oscillator, q is a measure for the oscillator strength, and A is a constant containing the sum of all the other oscillators. Nylon 11 film has the first absorption maximum at 215 nm due to the $n-\pi^*$ transition of carbonyl group in amide bonding. Figure 7 shows the plot of RI at wavelengths of 632.8 and 830 nm and the predicted curve of the wavelength dispersion of RI using eq 2 with $\lambda_0 = 215$ nm. RI values at 532 and 1064 nm obtained from the predicted plots are also listed in Table 1.

Second-Order Optical Nonlinearity. As described in the Experimental Section, SHG measurement was carried out for the sample films without DANS. SHG intensities of the sample films were measured by the Maker fringe analysis.[17,18] These measurements were made relative to a Y-cut quartz plate ($d_{11} = 1.2 \times 10^{-9}$ esu (=0.5 pm/V)) to determine SHG coefficients. In this technique, a plane sample was rotated in the path of a fundamental beam of wavelength of 1064 nm from a Q-switched Nd:YAG pulse laser. The second harmonic

power, $P_{2\omega}$, detected is given by

$$P_{2\omega} = \frac{512\pi^3}{A} t_\omega{}^4 T_{2\omega} \frac{d^2 p^2(\theta)}{(n_\omega{}^2 - n_{2\omega}{}^2)^2} P_\omega{}^2 \sin^2 \Psi \quad (3)$$

where A is the beam area, t_ω and $T_{2\omega}$ are the transmission factors for the incident fundamental and the second harmonic light, respectively, n_ω and $n_{2\omega}$ are the refractive indices of the incident fundamental and the second harmonic light, respectively, d is the second harmonic coefficient, $p(\theta)$ is the projection factor, P_ω is the incident fundamental laser power, and θ is the angle between the incident laser beam and the normal to the film being measured.

$$\Psi = \frac{\pi l}{2} \frac{4}{\lambda} (n_\omega \cos \theta_\omega - n_{2\omega} \cos \theta_{2\omega}) \quad (4)$$

where l is the film thickness, λ is the wavelength of the fundamental laser beam, θ_ω and and $\theta_{2\omega}$ are the angles of refraction at ω and 2ω, respectively, and

$$\sin \theta_\omega = (\sin \theta)/n_\omega, \sin \theta_{2\omega} = (\sin\theta)/n_{2\omega} \quad (5)$$

from Snell's law.

Transmission factors are defined as

$$t_\omega = \frac{2 \cos \theta}{n_\omega \cos \theta + \cos \theta_\omega} \quad (6)$$

for the p-polarized fundamental light,

$$t_\omega = \frac{2 \cos \theta}{n_\omega \cos \theta_\omega + \cos \theta} \quad (7)$$

for the s-polarized fundamental light, and

$$T_{2\omega} = 2n_{2\omega} \cos \theta_{2\omega} \frac{(n_\omega \cos \theta + \cos \theta_\omega)(n_{2\omega} \cos \theta_\omega + n_\omega \cos \theta_{2\omega})}{(n_{2\omega} \cos \theta + \cos \theta_{2\omega})^3} \quad (8)$$

for the p-polarized second harmonic light. The detailed description from eq 3 to eq 8 appeared in ref 18.

The poling process induces a polar axis in the poled polymer film. The axis is essentially an infinite-fold rotational axis with an infinite number of mirror planes.[19] Undrawn and poled polymers belong to the ∞mm point group. Drawn and poled polymers belong to the $mm2$ point group, where the symmetry operations include a 2-fold axis along the film normal direction and two mirror planes perpendicular to each other. In both cases, nonlinear polarization P_{NL} is given by

$$\boldsymbol{P}_{NL} = \begin{pmatrix} 0 & 0 & 0 & 0 & d_{15} & 0 \\ 0 & 0 & 0 & d_{24} & 0 & 0 \\ d_{31} & d_{32} & d_{33} & 0 & 0 & 0 \end{pmatrix} \begin{pmatrix} E_1^2 \\ E_2^2 \\ E_3^2 \\ 2E_2E_3 \\ 2E_1E_3 \\ 2E_1E_2 \end{pmatrix} \quad (9)$$

where there are five nonzero d coefficients. In the case of as-prepared undrawn and poled polymer, the equivalent relation between tensor components of

$$d_{31} = d_{32} = d_{24} = d_{15} \quad (10)$$

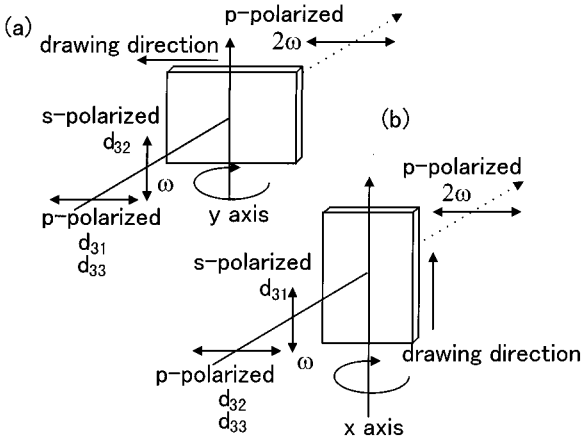

Figure 8. Schematic configuration of SHG measurements. Double-ended arrows represent the polarization of the wave.

can be obtained under the Kleinman symmetry restriction.[20] Thus second-order optical nonlinearity for as-prepared undrawn and poled polymer films can be characterized by two dependent d coefficients, d_{33} and d_{31}. In the poled random orientation of medium chains, the ratio of d_{33}/d_{31} is 3. On the contrary, drawn and poled polymer films have the tensor component relation of

$$d_{15} = d_{31}, d_{24} = d_{32} \quad (11)$$

under the Kleinman symmetry restriction.[20] The second-order optical nonlinearity for drawn and poled Nylon 11 films is characterized by three independent nonzero d coefficients, d_{33}, d_{32}, and d_{31}. The same type of tensor components was reported in drawn and poled PVDF[21,22] and polyurea.[23] As shown in Figure 8, the sample was set on the Maker fringe measurement system so that the drawing direction is parallel or perpendicular to the rotation axis for tilting the sample. The tensor components measured for each measurement mode are summarized in Figure 8. Therefore, in the case that rotation axis is perpendicular to the drawing direction in Figure 8a, projection factors are defined as

$$dp(\theta) = d_{33} \sin^2 \theta_\omega \sin \theta_{2\omega} + d_{31}(\cos^2 \theta_\omega \sin \theta_{2\omega} + 2 \cos \theta_\omega \sin \theta_\omega \cos \theta_{2\omega}) \quad (12)$$

for the p-polarized fundamental and p-polarized second harmonic light and

$$dp(\theta) = d_{32} \sin \theta_{2\omega} \quad (13)$$

for the s-polarized fundamental and p-polarized second harmonic light. Whereas, in the case where the rotation axis is parallel to the drawing direction in Figure 8b, projection factors are defined as

$$dp(\theta) = d_{33} \sin^2 \theta_\omega \sin \theta_{2\omega} + d_{32}(\cos^2 \theta_\omega \sin \theta_{2\omega} + 2 \cos \theta_\omega \sin \theta_\omega \cos \theta_{2\omega}) \quad (14)$$

for the p-polarized fundamental and p-polarized second harmonic light and

$$dp(\theta) = d_{31} \sin \theta_{2\omega} \quad (15)$$

for the s-polarized fundamental and p-polarized second harmonic light.

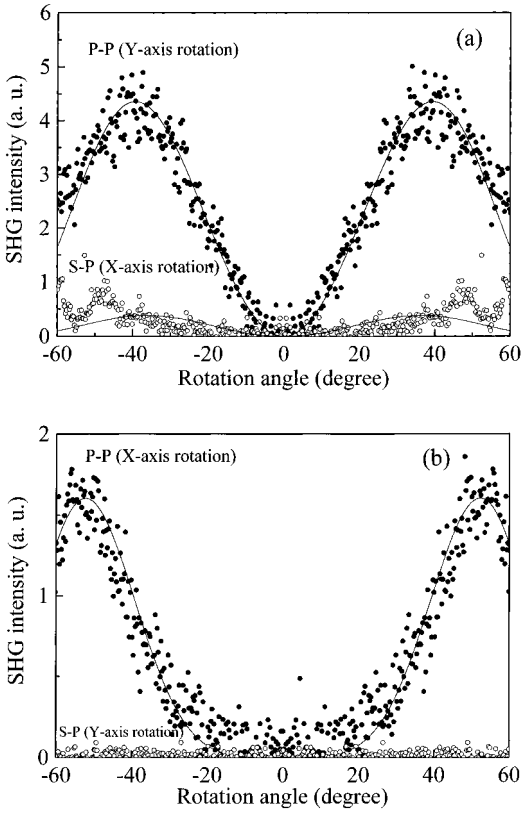

Figure 9. Typical Maker fringe patterns of the drawn and poled films. Solid curve is the theoretical plots with $n_\omega = 1.491$, $n_{2\omega} = 1.503$, and $l = 32.6\ \mu$m. Theoretical plots in part a give $d_{33} = 2.1 \times 10^{-9}$ esu and $d_{31} = 5.7 \times 10^{-10}$ esu and those in part b give $d_{33} = 2.0 \times 10^{-9}$ esu and $d_{32} \simeq 0$ esu.

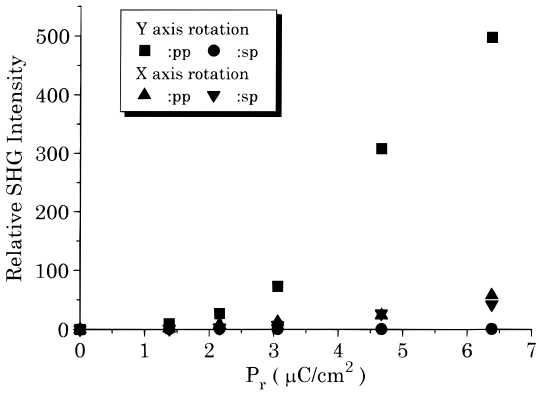

Figure 10. Relative SHG intensity plots vs P_r.

Typical Maker fringe patterns for a sample film with $P_r = 6.4\ \mu$C/cm^2 are shown in Figure 9. The solid curve in Figure 9 is the theoretical fitting using eq 3 with $n_\omega = 1.491$, $n_{2\omega} = 1.503$, and $l = 32.6\ \mu$m. Theoretical plots in Figure 9a give $d_{33} = 2.1 \times 10^{-9}$ esu and $d_{31} = 5.7 \times 10^{-10}$ esu and those in Figure 9b give $d_{33} = 2.0 \times 10^{-9}$ esu and $d_{32} \simeq 0$ esu. Figure 10 shows the relative SHG intensity measured at rotation angle of 50° plotted against corresponding P_r values. Each SHG intensity increases with increasing P_r value. Coherence length $l_c\ (=\lambda/[4|n_\omega - n_{2\omega}|])$ is calculated using refractive indices measured at 532 and 1064 nm. The coherence length along the drawing direction in the plane of polymer film l_{31} is 26.6 μm and that parallel to the poling direction l_{33} is 22.2 μm.

The value of d_{33} is calculated from both eqs 12 and 14, and the values are comparable to each other. In Figure 11, SHG coefficients d_{33}, d_{32}, and d_{31} are plotted

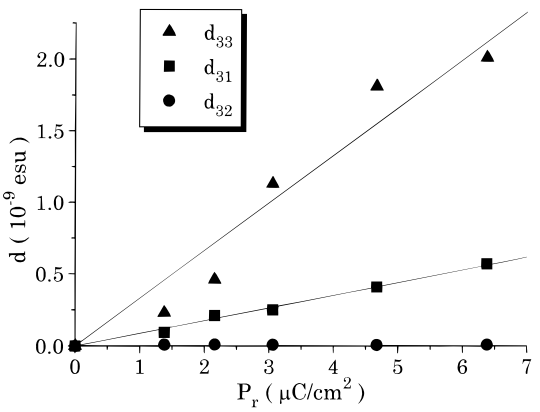

Figure 11. Plots of SHG coefficients, d_{33}, d_{32}, and d_{31}, vs P_r.

as a function of P_r value. The values of d_{33} and d_{31} proportionally increase with increasing P_r value. Good correlation between the d value and P_r implies that the second-order optical nonlinearity originates from the noncentrosymmetrically aligned polar crystallite dipoles, which are also responsible for the significant polarization reversal and remanent polarization. The obtained d_{33} value of $(2.0-2.1) \times 10^{-9}$ esu at $P_r = 6.4\ \mu$C/cm^2 is comparable to d_{33} of 3.2×10^{-9} esu for fully polarized P(VDF-TrFE).[9] The value of d_{33} is the largest d coefficient, which means that dipole moments largely align along the poling direction (z direction in Figure 6). The average ratio $d_{33}/d_{31} = 3.8$ is obtained, whereas d_{32} value is nearly zero irrespective of the P_r value. These results imply that the sample film is anisotropic. SHG coefficients of d_{33}(PVDF) = $2d_{31}$(PVDF) = d_{11}(quartz), and d_{32}(PVDF) = 0 were measured for drawn and poled PVDF films,[21,22] which also have the $mm2$ point group. The proportionality between the d_{33} value and P_r was also reported for P(VDF-TrFE).[24]

Conclusion

The internal electric field and second-order optical nonlinearity were investigated for cold-drawn and poled Nylon 11 films. Both physical values are related well to the remanent polarization determined by the polarization reversal. Second-order optical nonlinearity can be expressed by three different tensor components, d_{33}, d_{32}, and d_{31}. Further interesting study of the dependence of these values on drawing ratio is in progress.

Acknowledgment. N.T. gratefully acknowleges Drs. G. Thomas Davis, Aime S. DeReggi, and Michael Schen, Polymer Division, National Institute of Standards & Technology, for fruitful discussions and comments.

References and Notes

(1) Furukawa, T.; Date, M.; Fukada, E. *J. Appl. Phys.* **1980**, *51*, 1135.
(2) Furukawa, T.; Lovinger, A. J.; Davis, G. T.; Broadhurst, M. G.; *Macromolecules* **1983**, *16*, 1885.
(3) Lee, J. W.; Takase, Y.; Newman, B. A.; Scheinbeim, J. I. *J. Polym. Sci. Part B, Polym. Phys.* **1991**, *29*, 273.
(4) Lee, J. W.; Takase, Y.; Newman, B. A.; Scheinbeim, J. I. *J. Polym. Sci. Part B, Polym. Phys.* **1991**, *29*, 279.
(5) Murata, Y.; Tsunashima, K.; Koizumi, N.; Ogami, K.; Hosokawa, F.; Yokoyama, K. *Jpn. J. Appl. Phys.* **1993**, *32*, L849.
(6) Tsutsumi, N.; Iyo, T.; Sakai, W.; Kiyotsukuri, T. *Macromolecules* **1996**, *29*, 8883.
(7) Tsutsumi, N.; Davis, G. T.; DeReggi, A. *Macromolecules* **1991**, *24*, 6392.
(8) Tsutsumi, N.; Ueda, Y.; Kiyotsukuri, T.; DeReggi, A. S.; Davis, G. T. *J. Appl. Phys.* **1993**, *74*, 3366.

(9) Tsutsumi, N.; Ono, T.; Kiyotsukuri, T. *Macromolecules* **1993**, *26*, 5447.
(10) Tsutsumi, N.; Fujii, I.; Ueda, Y.; Kiyotsukuri, T. *Macromolecules* **1995**, 28, 950.
(11) Bauer, F.; *Ferroelectrics* **1983**, *49*, 231.
(12) Bur, A. J.; Roth, S. C. Preparation of Thin Film Polyvinylidene Fluoride Shock Wave Pressure Transducers. Interagency Report 87-3680; NTIS PB881560070; U.S. National Bureau of Standards: Washington, DC, 1987.
(13) Balizer, E.; Fedderly, J.; Haught, D.; Dickens, B.; DeReggi, A. S. *J. Polym. Sci. Part B, Polym. Phys.* **1994**, *32*, 365.
(14) Liptay, W. In *Exited States Vol I*; Lim, E. C., Ed.; Academic Press: New York and London, 1974; pp 129−229.
(15) Havinga, E. E.; van Pelt, P. *Ber. Bunsen-Ges. Phys. Chem.* **1979**, *83*, 816.
(16) Sears. F. W. *Electricity and Magnetism*; Addison-Wesley Press: Cambridge, MA, 1951; pp 176−178.
(17) Maker, P. D.; Terhune, R. W.; Nisenoff, M; Savage, C. M. *Phys. Rev. Lett.* **1962,** *8*, 21.
(18) Jerphagnon, J.; Kurtz, S. K. *J. Appl. Phys.* **1970**, *40*, 1667.
(19) Prasad, P. N.; Williams, D. J. *Introduction to Nonlinear Optical Effects in Molecules Polymers*; Wiley-Interscience: New York, 1991; Chapter 4, pp 66−73.
(20) Kleinman, D. A. *Phys. Rev.* **1962**, *126*, 1977.
(21) Bergman, Jr. J. G.; McFee, J. H.; Crane, G. R. *Appl. Phys. Lett.* **1971**, *18*, 203.
(22) McFee, J. H.; Bergman, J. G.; Crane G. R. *Ferroelectrics* **1972**, *3*, 305.
(23) Watanabe, T.; Tao, X. T.; Kim, J.; Miyata, S.; Nalwa, H. S.; Lee, S. C. *Nonlinear Opt.* **1996**, *15*, 327.
(24) Wicker, A.; Berge, B.; Lajzerowicz, J.; Legrand, J. F. *J. Appl. Phys.* **1989**, *66*, 342.

MA9613852